

Characteristic Euler shock-fitting formulation for multi-dimensional flows

Ertugrul A. Basesme^{1,*,\dagger,\ddagger}, I. Sinan Akmandor^{2,\S} and Ahmet S. Ucer^{3,\S}

¹*Punto Engineering Ltd., 06510, Ankara, Turkey*

²*Middle East Technical University, Aerospace Eng. Dept., 06531, Ankara, Turkey*

³*Middle East Technical University, Mechanical Eng. Dept., 06531, Ankara, Turkey*

SUMMARY

A three-dimensional explicit time marching algorithm has been developed for the numerical solution of inviscid internal flows. The formulation uses the natural streamline co-ordinate system. The unsteady Euler equations in non-conservative form are expressed in terms of the extended Riemann variables and the flow angles. Along the characteristic trajectories in the space–time domain, these equations reduce to a system of ordinary differential equations. Boundary conditions are also implemented in characteristic form. Shock waves are calculated after performing a one-point shock correction that maintains conservation across the discontinuity.

The algorithm has been applied to subsonic, transonic and supersonic test cases. Despite the wide range in the Mach number and the diversity of the tested flow geometries, close agreement have been obtained with available analytical and numerical results. Copyright © 2003 John Wiley & Sons, Ltd.

KEY WORDS: Euler solver; finite difference; time-marching; characteristic method; three-dimensional flow

1. INTRODUCTION

Flows with high Reynolds numbers are essentially dominated by convective effects and the free stream properties can be calculated using the conservative Euler equations which resolve rotationality, shock waves and contact discontinuities. Traditional finite difference Euler schemes that are based on fixed stencil interpolations, solve the conservative flow equations and capture shocks. However, fixed stencil interpolation of second or higher order accuracy is necessarily oscillatory near a discontinuity. In 1970s and early 1980s, various methods incorporating artificial viscosity have been developed to damp out these oscillations. Later, limiters were applied to eliminate oscillations. However, the order of accuracy of the interpolation near the discontinuity necessarily degenerates to first order near smooth extrema [1]. Shock fitting

*Correspondence to: E. A. Basesme, Emek Mah. 77 Sok. Saha Apt., 1/1 No.1 06510, Ankara, Turkey.

^{\dagger}E-mail: eb@punto.com.tr

^{\ddagger}Director.

^{\S}Professor.

techniques suitable for high-speed flows were also developed. Shock fitting techniques makes special treatment for explicitly computing discontinuities and inaccuracies due to shock smearing are eliminated. The shock position and strength are calculated from the Rankine–Hugoniot relations. If shocks are tracked, the equations need not be in conservative form. The method of characteristics for hyperbolic equations is the natural choice for numerical computation as the calculation node points lie along the ‘characteristics’. There are many classical choice of network configuration associated with three-dimensional flow equations solved by the methods of characteristics. Tetrahedral characteristic line and surface networks of Thornhill [2] and the prismatic network of bicharacteristics of Holt [3] are to name a few. To fulfill the stability criterion, the domain of dependence of these characteristic difference schemes must contain the domain of dependence of the differential equations. This task has been greatly simplified in the present algorithm as the streamline position and flow properties are calculated along local time–space characteristics.

Method of characteristics can be used with a shock-patching procedure where the shock build-up is indicated by a crossing of characteristics of the same family. Many successful shock fitting methods exist. Moretti’s method [4] is a transient method based on characteristics calculations of the moving shock wave. Eaton [5] applies this method to three-dimensional flow with good accuracy. Another characteristic approach in resolving discontinuity in an Eulerian mesh is the use of an ‘inverse marching method’. The present method falls into this category and uses the quasi-one-dimensional characteristic forms of the Euler equations with a shock-fitting calculation. Accordingly, the location of the solution points are specified *a priori*. The three characteristics at the solution node are extended rearward to intersect a plane on which are located initial data points from previous calculation. The only reduction in accuracy stems from the interpolation of calculated flow properties along the initial streamline. The quasi-one-dimensional formulation of the Euler equations were rigorously described in 1984 [6]. Even though conservative variables were not used, highly accurate solutions were obtained. The formulation was employed to solve the flow properties in wave rotor applications [7, 8]. Time accurate solutions were obtained, where shocks and contact discontinuities were tracked and corrected explicitly. The formulation was also shown to be suitable to supersonic/hypersonic analysis of flow fields with predominantly oblique shocks [9].

The present work is a development and application of Verhoff’s formulation to multi-dimensional internal flows. The method was validated by comparison with analytic and numerical solutions. Firstly, a single diaphragm shock tube problem is solved to show the code’s transient solution capability. Secondly, transonic quasi-one-dimensional Laval nozzle flow is solved. Then, subsonic two-dimensional sinusoidal bump duct flow solutions have been obtained. Finally, the solutions of a three-dimensional supersonic flow with an angle of attack, entering a simple constant area duct have been obtained.

2. THREE-DIMENSIONAL CHARACTERISTIC EULER EQUATIONS

The following governing equations of motion describe the high-speed internal flow of an unsteady, inviscid, adiabatic, compressible ideal gas with respect to a stationary reference frame. The three-dimensional Euler equations are written in terms of extended Riemann variables in a natural streamline co-ordinate system (s, m, n) . As a result, Euler equations become a quasi-one-dimensional system, regardless of the number of spatial dimensions. The time step

is determined by the CFL criteria, as to assure the numerical stability of the scheme. Accordingly, the initial data points 1, 2, 3 (Figure 2) always lie within the zone of dependence of the solution point at a new time step and no explicit numerical dissipation or smoothing is required to further enhance the stability of the solution. Subsonic, transonic and supersonic flows can be handled equally well. The extension of the method can be evaluated for the solution of the Navier–Stokes equations, which would require inclusion of addition source terms in Equations (1)–(5).

$$Q_t + (q + a)Q_s = -\frac{\gamma - 1}{2} a \left(S - \frac{2}{\gamma - 1} \right) \frac{\partial}{\partial s} \left(q - \frac{2}{\gamma - 1} a \right) - \frac{\gamma - 1}{2} qaS(\theta_n + \phi_m \cos \theta) \quad (1)$$

$$R_t + (q - a)R_s = +\frac{\gamma - 1}{2} a \left(S - \frac{2}{\gamma - 1} \right) \frac{\partial}{\partial s} \left(q + \frac{2}{\gamma - 1} a \right) + \frac{\gamma - 1}{2} qaS(\theta_n + \phi_m \cos \theta) \quad (2)$$

$$S_t + qS_s = 0 \quad (3)$$

$$\theta_t + q\theta_s = -\frac{a^2}{\gamma q} P_n \quad (4)$$

$$\phi_t + q\phi_s = -\frac{a^2}{\gamma q \cos \theta} P_m \quad (5)$$

where, the velocity magnitude and speed of sound are denoted by q and a , respectively, and P is the logarithm of pressure. The extended Riemann variables Q and R are defined as

$$Q \equiv q + aS \quad (6)$$

$$R \equiv q - aS \quad (7)$$

while the modified entropy is defined in terms of pressure p and density ρ as

$$S \equiv \frac{1}{\gamma(\gamma - 1)} [2\gamma - \ln(p/\rho^\gamma)] \quad (8)$$

The flow angles θ and ϕ and the streamline co-ordinate system are defined in Figure 1. Time is denoted by t , while distances along and normal to the streamline direction are denoted by the vectors s , m and n , respectively. The n direction lies in the plane defined by the y -axis and the angle ϕ ; the m direction is normal to this plane.

The flux vector splitting procedure of Reference [10] is used to distinguish directions of propagation normal to the local streamline direction. The three-dimensional equation in matrix form is

$$\frac{\partial}{\partial t} \{F\} + [A] \frac{\partial}{\partial s} \{F\} + [B] \frac{\partial}{\partial n} \{F\} + [C] \frac{\partial}{\partial m} \{F\} = \{0\} \quad (9)$$

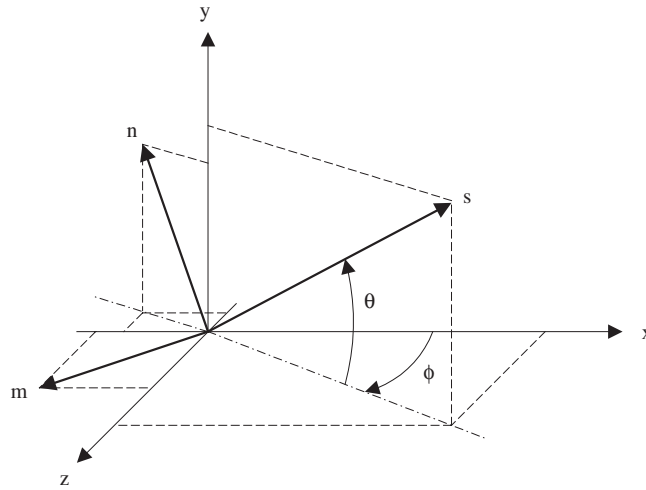


Figure 1. Definition of flow angles and streamline co-ordinate system.

where

$$\{F\} = \{Q \ R \ \theta \ \phi\}^T \quad (10)$$

and $[A]$ is the diagonal matrix of characteristic velocities

$$[A] = \begin{bmatrix} q+a & 0 & 0 & 0 \\ 0 & q-a & 0 & 0 \\ 0 & 0 & q & 0 \\ 0 & 0 & 0 & q \end{bmatrix} \quad (11)$$

$[A]$ matrix is composed of eigenvalues along the diagonal. $[B]$ and $[C]$ matrices are written as

$$[B] = \begin{bmatrix} 0 & 0 & qa & 0 \\ 0 & 0 & -qa & 0 \\ \frac{a}{2q} & -\frac{a}{2q} & 0 & 0 \\ 0 & 0 & 0 & 0 \end{bmatrix} \quad (12)$$

$$[C] = \begin{bmatrix} 0 & 0 & 0 & qa \cos q \\ 0 & 0 & 0 & qa \cos q \\ 0 & 0 & 0 & 0 \\ \frac{a}{2q \cos q} & -\frac{a}{2q \cos q} & 0 & 0 \end{bmatrix} \quad (13)$$

$[B]$ matrix related to normal direction n and can be transformed in characteristic directions:

$$[B] = [X]^{-1}[\lambda_B][X] \quad (14)$$

where $[\lambda_B]$ matrix is composed of eigenvalues normal to the streamline direction.

$$[\lambda_B] = \begin{bmatrix} 0 & 0 & 0 & 0 \\ 0 & 0 & 0 & 0 \\ 0 & 0 & -a & 0 \\ 0 & 0 & 0 & a \end{bmatrix} \quad (15)$$

Using Equations (12), (14) and (15), the matrix $[X]$ (is determined and the $[B]$ matrix is split into two parts as

$$[B] = [B^+] + [B^-] \quad (16)$$

where $[B^+]$ and $[B^-]$ correspond to the positive and negative eigenvalues, respectively

$$[B^+] = \begin{bmatrix} \frac{a}{4} & \frac{-a}{4} & 0 & \frac{qa}{2} \\ \frac{-a}{4} & \frac{a}{4} & 0 & \frac{qa}{2} \\ 0 & 0 & 0 & 0 \\ \frac{a}{4q} & \frac{-a}{4q} & 0 & \frac{a}{2} \end{bmatrix} \quad (17)$$

$$[B^-] = \begin{bmatrix} \frac{-a}{4} & \frac{a}{4} & 0 & \frac{qa}{2} \\ \frac{a}{4} & \frac{-a}{4} & 0 & \frac{-qa}{2} \\ 0 & 0 & 0 & 0 \\ \frac{a}{4q} & \frac{-a}{4q} & 0 & \frac{-a}{2} \end{bmatrix} \quad (18)$$

Similarly, the matrix $[C]$ related to the co-normal direction m , is split as

$$[C] = [C^+] + [C^-] \quad (19)$$

where

$$[C^+] = \begin{bmatrix} \frac{a}{4} & \frac{-a}{4} & 0 & \frac{qa \cos \theta}{2} \\ \frac{-a}{4} & \frac{a}{4} & 0 & \frac{-qa \cos \theta}{2} \\ 0 & 0 & 0 & 0 \\ \frac{a}{4q \cos \theta} & \frac{-a}{4q \cos \theta} & 0 & \frac{a}{2} \end{bmatrix} \quad (20)$$

$$[C^-] = \begin{bmatrix} \frac{-a}{4} & \frac{a}{4} & 0 & \frac{qa \cos \theta}{2} \\ \frac{a}{4} & \frac{-a}{4} & 0 & \frac{-qa \cos \theta}{2} \\ 0 & 0 & 0 & 0 \\ \frac{a}{4q \cos \theta} & \frac{-a}{4q \cos \theta} & 0 & \frac{-a}{2} \end{bmatrix} \quad (21)$$

The system of equations for 3D isentropic flow thus becomes

$$Q_t + (q+a)Q_s = -\frac{a}{4} \left[\frac{\partial}{\partial n} (Q-R)^+ - \frac{\partial}{\partial n} (Q-R)^- + \frac{\partial}{\partial m} (Q-R)^+ - \frac{\partial}{\partial m} (Q-R)^- \right] - \frac{qa}{2} \left[\left(\frac{\partial \theta^+}{\partial n} + \frac{\partial \theta^-}{\partial n} \right) + \cos \theta \left(\frac{\partial \phi^+}{\partial m} + \frac{\partial \phi^-}{\partial m} \right) \right] \quad (22)$$

$$R_t + (q-a)R_s = \frac{a}{4} \left[\frac{\partial}{\partial n} (Q-R)^+ - \frac{\partial}{\partial n} (Q-R)^- + \frac{\partial}{\partial m} (Q-R)^+ - \frac{\partial}{\partial m} (Q-R)^- \right] + \frac{qa}{2} \left[\left(\frac{\partial \theta^+}{\partial n} + \frac{\partial \theta^-}{\partial n} \right) + \cos \theta \left(\frac{\partial \phi^+}{\partial m} + \frac{\partial \phi^-}{\partial m} \right) \right] \quad (23)$$

$$\theta_t + q\theta_s = -\frac{a}{4q} \left[\frac{\partial}{\partial n} (Q-R)^+ + \frac{\partial}{\partial n} (Q-R)^- \right] - \frac{a}{2} \left(\frac{\partial \theta^+}{\partial n} - \frac{\partial \theta^-}{\partial n} \right) \quad (24)$$

$$\phi_t + q\phi_s = -\frac{a}{4q \cos \theta} \left[\frac{\partial}{\partial m} (Q-R)^+ + \frac{\partial}{\partial m} (Q-R)^- \right] - \frac{a}{2} \left(\frac{\partial \phi^+}{\partial m} - \frac{\partial \phi^-}{\partial m} \right) \quad (25)$$

where, $(\partial/\partial n)()^+$ and $(\partial/\partial n)()^-$ are one sided-derivatives along n , corresponding to the positive and negative eigenvalues normal to the streamline direction, respectively. Along m , $(\partial/\partial m)()^+$ and $(\partial/\partial m)()^-$ derivatives have similar meaning.

The flow variables are non-dimensionalized with respect to far-field conditions.

3. SOLUTION METHOD

Each equation in the system (Equations (22)–(25)) has the general form

$$\frac{\partial w}{\partial t} + \lambda \frac{\partial w}{\partial s} = z \quad (26)$$

where

$$\lambda = \begin{bmatrix} q + a & 0 & 0 & 0 & 0 \\ 0 & q - a & 0 & 0 & 0 \\ 0 & 0 & q & 0 & 0 \\ 0 & 0 & 0 & q & 0 \\ 0 & 0 & 0 & 0 & q \end{bmatrix} \tag{27}$$

$$w = \begin{pmatrix} Q \\ R \\ S \\ \theta \\ \phi \end{pmatrix} \tag{28}$$

$$z = \begin{bmatrix} -\frac{a}{4}[(Q - R)_n^+ - (Q - R)_n^- + (Q - R)_m^+ - (Q - R)_m^-] - \frac{qa}{2}[(\theta_n^+ + \theta_n^-) + \cos \theta(\phi_m^+ + \phi_m^-)] \\ \dots \\ \frac{a}{4}[(Q - R)_n^+ - (Q - R)_n^- + (Q - R)_m^+ - (Q - R)_m^-] + \frac{qa}{2}[(\theta_n^+ + \theta_n^-) + \cos \theta(\phi_m^+ + \phi_m^-)] \\ \dots \\ 0 \\ \dots \\ -\frac{a}{4q}[(Q - R)_n^+ + (Q - R)_n^-] - \frac{a}{2}[\theta_n^+ - \theta_n^-] \\ \dots \\ -\frac{a}{4q \cos \theta}[(Q - R)_m^+ + (Q - R)_m^-] - \frac{a}{2}[\phi_m^+ - \phi_m^-] \end{bmatrix} \tag{29}$$

In the $s-t$ plane, the characteristic equation is

$$\frac{ds}{dt} = \lambda, \quad \lambda = q \pm a, q \tag{30}$$

and the compatibility equations are:

$$\frac{dQ}{dt} = z_1 \quad \text{along} \quad \frac{ds}{dt} = q + a \tag{31}$$

$$\frac{dR}{dt} = z_2 \quad \text{along} \quad \frac{ds}{dt} = q - a \tag{32}$$

$$\frac{dS}{dt} = z_3 \quad \text{along} \quad \frac{ds}{dt} = q \tag{33}$$

$$\frac{d\theta}{dt} = z_4 \quad \text{along} \quad \frac{ds}{dt} = q \quad (34)$$

$$\frac{d\phi}{dt} = z_5 \quad \text{along} \quad \frac{ds}{dt} = q \quad (35)$$

where

$$z_1 = -\frac{a}{4} [(Q - R)_n^+ - (Q - R)_n^- + (Q - R)_m^+ - (Q - R)_m^-] - \frac{qa}{2} [(\theta_n^+ + \theta_n^-) + \cos \theta (\phi_m^+ + \phi_m^-)] \quad (36)$$

$$z_2 = \frac{a}{4} [(Q - R)_n^+ - (Q - R)_n^- + (Q - R)_m^+ - (Q - R)_m^-] + \frac{qa}{2} [(\theta_n^+ + \theta_n^-) + \cos \theta (\phi_m^+ + \phi_m^-)] \quad (37)$$

$$z_3 = 0 \quad (38)$$

$$z_4 = -\frac{a}{4q} [(Q - R)_n^+ + (Q - R)_n^-] - \frac{a}{2} [\theta_n^+ - \theta_n^-] \quad (39)$$

$$z_5 = -\frac{a}{4q \cos \theta} [(Q - R)_m^+ + (Q - R)_m^-] - \frac{a}{2} [\phi_m^+ - \phi_m^-] \quad (40)$$

Using an inverse marching procedure, these ordinary differential equations are integrated along the characteristic trajectories to calculate the flow variables (Q, R, S, θ and ϕ) at the next time level.

This procedure is repeated until convergence. The error term checked for convergence is determined by calculating the maximum change in pressure between two consecutive time levels.

$$\text{error} = \max \left| \frac{P_{i,j,k}^{n+1} - P_{i,j,k}^n}{P_{i,j,k}^n} \right| \begin{matrix} i = 1 \rightarrow imx \\ j = 1 \rightarrow jmx \\ k = 1 \rightarrow kmx \end{matrix} \quad (41)$$

4. INVERSE MARCHING, SHOCK FITTING AND DISCRETIZATION

The three characteristics lines intersecting a computational node, are extended rearward to intersect the streamline which passes through the same point in the previous time t . For two- and three-dimensional flows, the characteristic trajectories in space-time domain are shown in Figures 2 and 3, respectively. The Courant-Friedrichs-Lewy (CFL) stability criterion is used in evaluating the local time step.

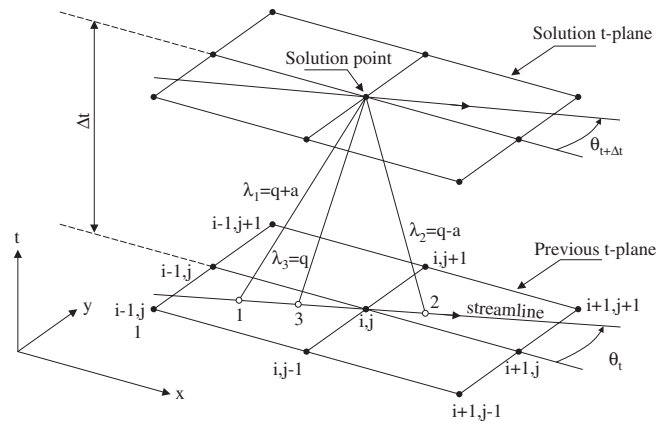


Figure 2. Characteristic trajectories in the space-time domain (2D).

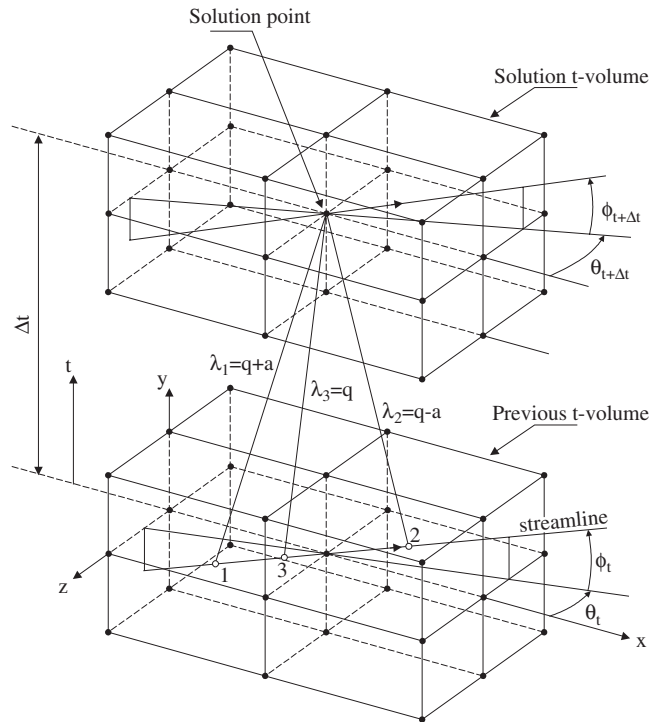


Figure 3. Characteristic trajectories in the space-time domain (3D).

The time step, Δt , is determined using the CFL condition which requires the domain of dependence of the numerical approximation to include the domain of dependence of the differential equations. The maximum time step is calculated using

$$\max(\Delta t) = \text{CFL} \frac{\max(\Delta x)}{\min |q + a|} \quad (42)$$

The time step, Δt , can be calculated either for each individual node, or for the entire computational domain. The former method is called the 'local maximum time stepping' where the latter is called the 'global maximum time stepping'. If local maximum time stepping is used, the solution over the whole domain is not time accurate, but convergence to steady state is faster.

CFL numbers less than 1.0 results in convergence, where CFL number larger than 1.0 trigger instabilities and the solution diverges.

Shock treatment starts with identifying the intervals or cells where compressions of sufficient strength are located. Using an iterative procedure, the shock velocity is calculated and the unsteady problem is transformed into a steady one with respect to the shock speed. Then, normal shock relations are used to calculate the flow variables downstream of the shock. The shock location is tracked in time and the flow variables at the nodes downstream of the shock are calculated using the shock fitting technique of Moretti [11].

After each iteration, a shock correction based on mass, momentum and energy conservation is applied. This procedure removes the shock jump errors and force the shock wave to the correct location.

The concept of shock correction used in one-dimensional flows is also applicable in problems involving two- or three-dimensional flows. Since the formulation is based on a quasi-one-dimensional flow, information about the orientation of the shock normal is necessary. Similar to that of Moretti [11] the shock correction process is started by evaluating a shock parameter, Σ for every possible pair of neighbouring grid points. If Σ exceeds some threshold, the interval is marked as having a shock fragment.

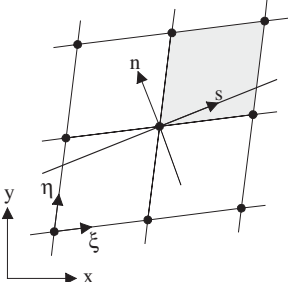
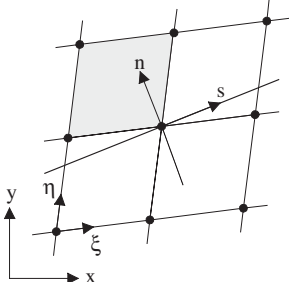
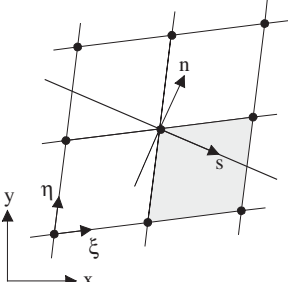
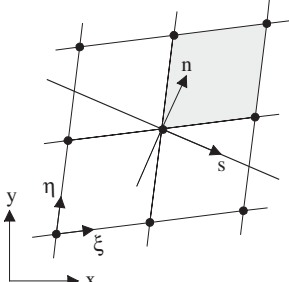
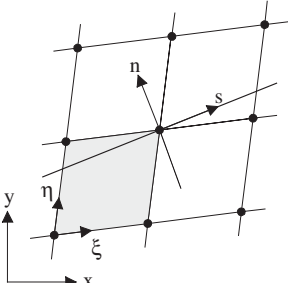
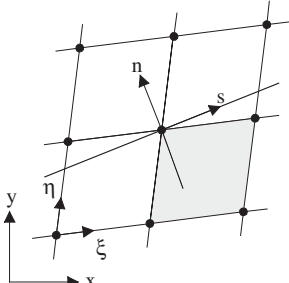
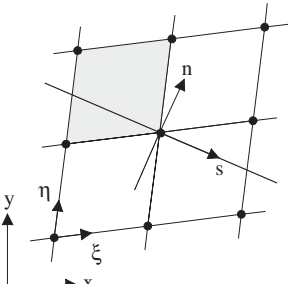
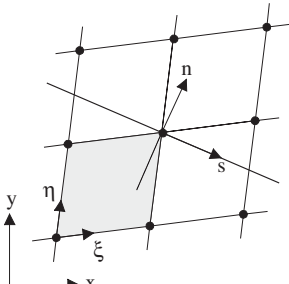
The velocity components normal to the shock wave are calculated. Using the normal velocity components and normal shock relations, shock jump errors are eliminated.

Although shock fitting in one-dimensional and multi-dimensional flows are handled in a similar fashion, book-keeping required for shock fitting in multi-dimensional flows is relatively cumbersome.

The local source terms z (the right-hand side of Equation (26)), the independent variables w (i.e. Q, R, S, θ and ϕ) and the dependent variables q at the new time level are evaluated using the former flow parameters at points 1, 2, 3. Streamwise spatial derivative, $\partial w / \partial s$, and the derivatives normal to the streamline direction, $\partial w / \partial n$ and $\partial w / \partial m$, are discretized with one sided differences in a manner consistent with the physical direction of wave propagation. If the flow is supersonic, streamwise derivatives of all the flow variables are calculated using backward differencing. If the flow is subsonic, $\partial R / \partial s$ is calculated using forward differencing and the rest of the streamwise derivatives are calculated using backward differencing.

For a 2D flow, the computational cells used in the calculation of the $\partial w / \partial s$ and $\partial w / \partial n$ derivatives are shown in Table I as shaded regions.

Table I. Computational cells used in calculating streamwise and normal derivatives.

	$\frac{\partial w}{\partial s}$	$\frac{\partial w}{\partial n}$
FORWARD DIFFERENCE		
		
BACKWARD DIFFERENCE		
		

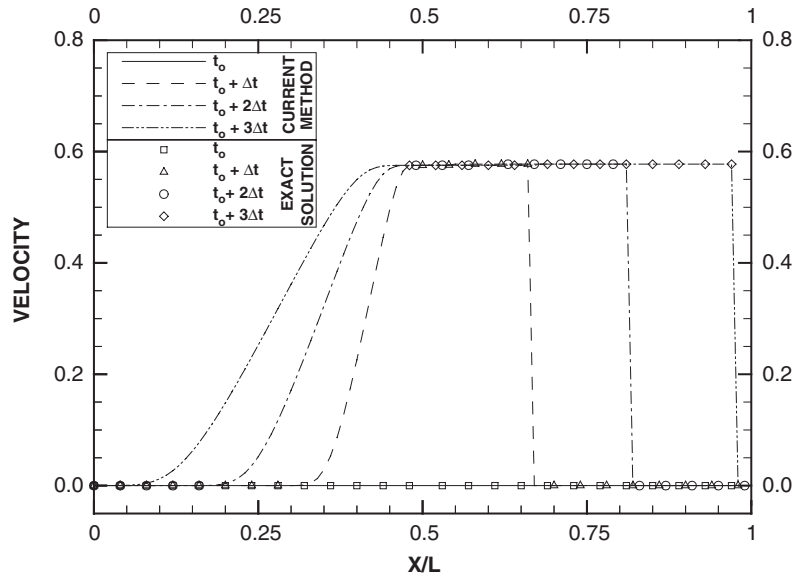


Figure 4. Evolution of velocity distribution.

5. RESULTS AND DISCUSSION

5.1. One-dimensional shock tube problem

Classical shock tube problem is solved, since it is a good test problem for high-speed compressible flow with unsteady wave propagation.

The shock tube is divided into 100 equal spatial intervals. Initially the gas is at rest at constant temperature with a pressure ratio of 5:1 across the diaphragm which is located in the middle of the tube. After the diaphragm is ruptured, the contact surface and the shock wave are tracked and a one point shock correction is applied after each iteration.

CFL number was 0.99, where the shock reached the end of the tube in about 60 iterations.

The unsteady wave propagation is shown in Figures 4–7 using the plots of velocity, modified entropy, pressure and density distributions. Step discontinuities at the contact surface and the shock wave are evident. As expected, across the shock velocity, modified entropy, pressure and density change discontinuously. On the other hand, across the contact surface modified entropy and density change discontinuously whereas velocity and pressure are continuous. The propagation of shock and contact surface is plotted in Figure 8 and the results are in good agreement with the exact solution.

5.2. Transonic Laval nozzle (Q1D)

The transonic flow in a converging–diverging nozzle is solved to demonstrate the accuracy of the code for a quasi one-dimensional flow. The geometry of the nozzle is given by the

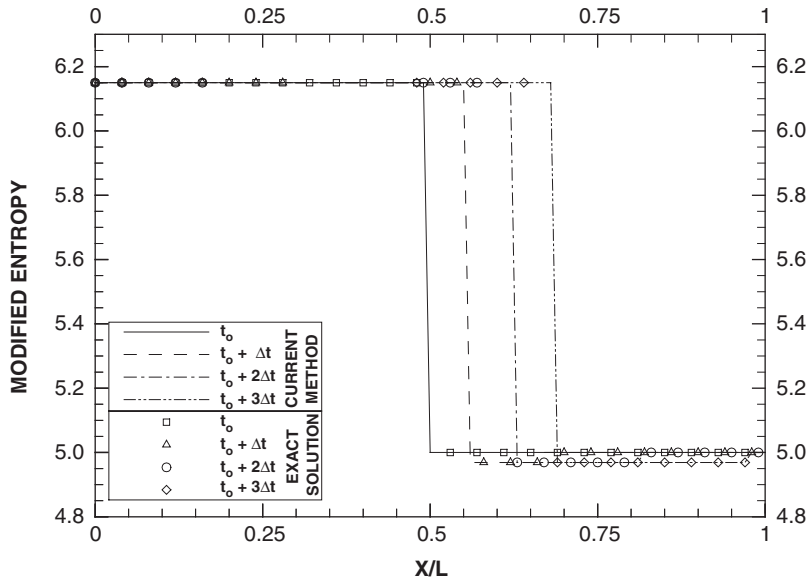


Figure 5. Development of entropy distribution.

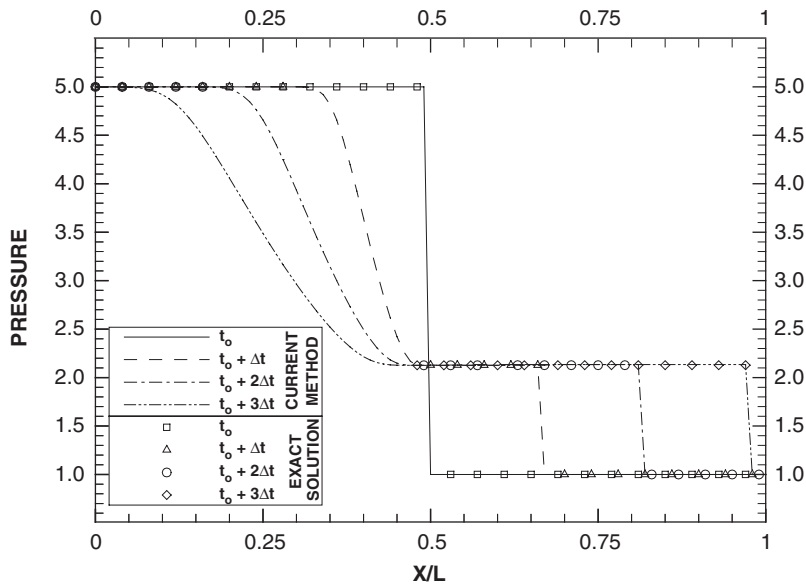


Figure 6. Evolution of pressure distribution.

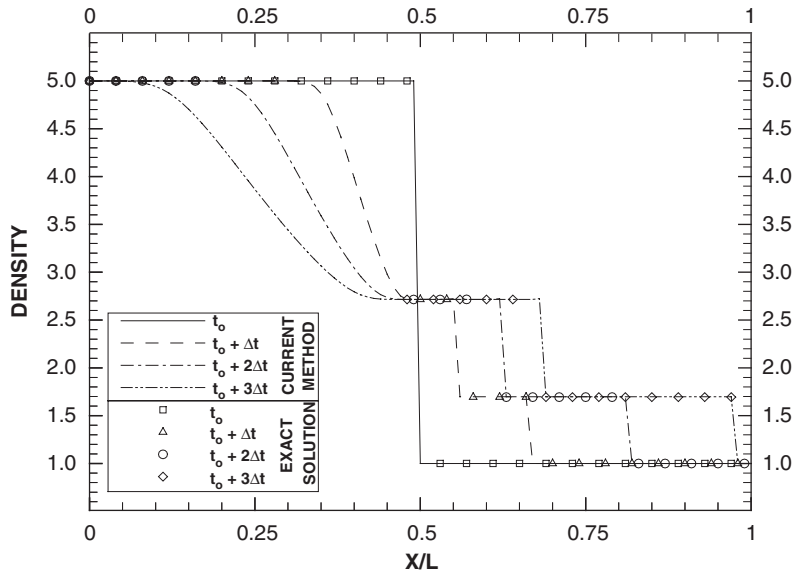


Figure 7. Evolution of density distribution.

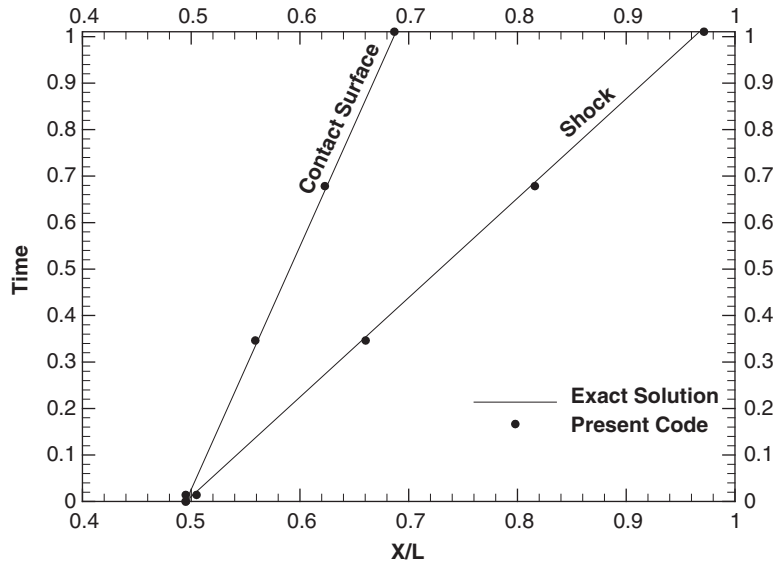


Figure 8. Shock and contact surface location in time.

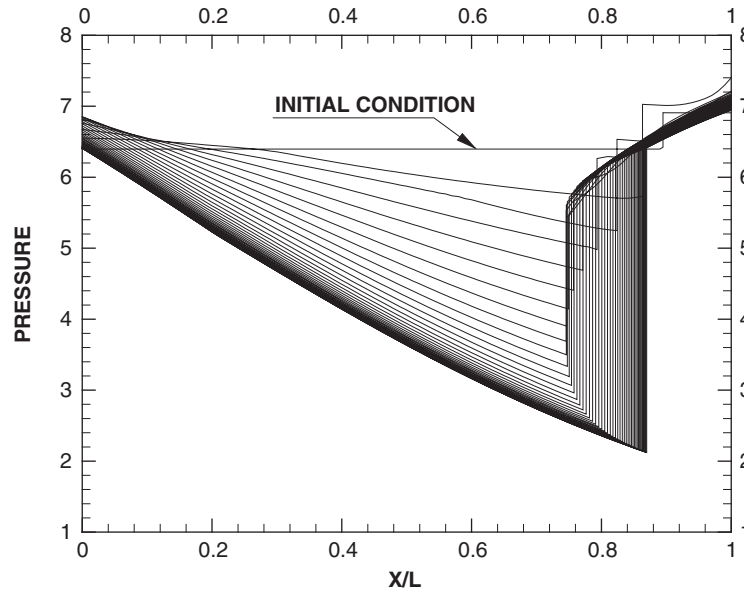


Figure 9. Unsteady evolution of the flow.

following expressions:

$$0 \leq x \leq 2 \quad A(x) = 1 + 0.033333(1 - 0.5x)^2$$

$$2 \leq x \leq 10 \quad A(x) = 1 + 0.027083(1 - 0.5x)^2$$

Note that the throat is at $x/L = 0.2$. Following boundary conditions are used

$$p_{\text{in}} = 6.40, \quad p_{\text{out}} = 6.91$$

$$T_{\text{in}} = 0.90, \quad T_{\text{out}} = 0.96$$

$$\rho_{\text{in}} = 7.07, \quad \rho_{\text{out}} = 7.17$$

$$u_{\text{in}} = 0.77, \quad u_{\text{out}} = 0.55$$

Initially the nozzle is assumed to be separated by a diaphragm placed at $x/L = 0.9$. Initially the pressure and density ratio across the diaphragm are assumed to be 6.40/6.91 and 7.07/7.17, respectively. Initially the gas on both sides is assumed to have flow velocities of 0.77 and 0.55. These unrealistic initial conditions are specified to see the robustness of the code. After the diaphragm is ruptured, the discontinuity is tracked and a one point shock correction is performed after each iteration. The unsteady evolution of the flow in the nozzle is illustrated in Figure 9 where CFL number was 0.99.

Steady state pressure, density and Mach number distribution along the nozzle are given in Figures 10–12 together with the analytical solution. Numerical and analytical results are in excellent agreement. Steady state shock location and the discontinuity magnitude across the shock are predicted accurately.

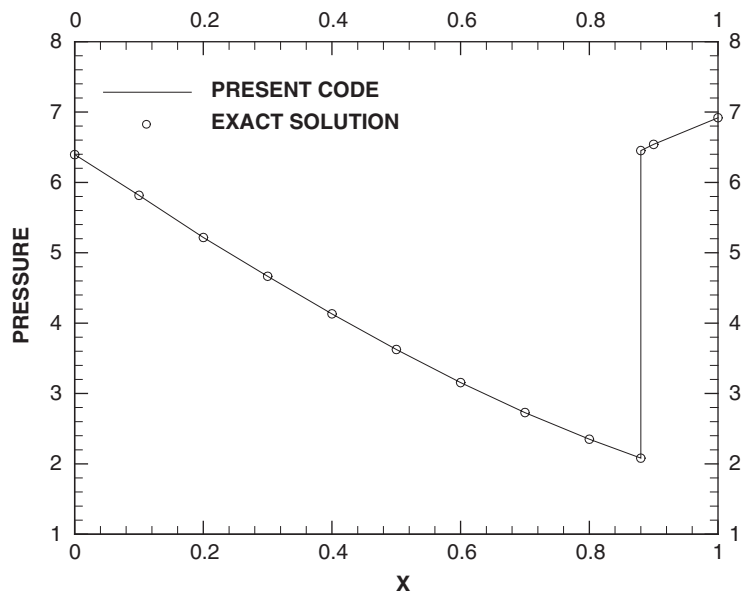


Figure 10. Steady state pressure distribution along the converging–diverging nozzle.

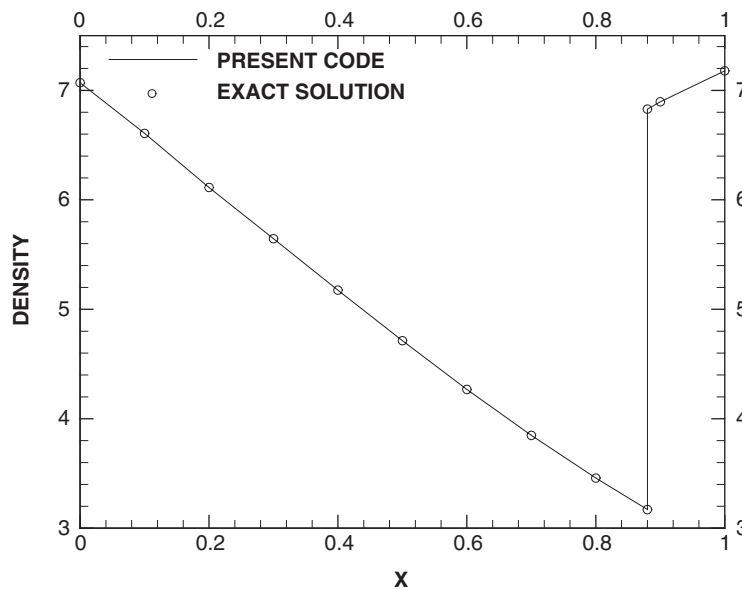


Figure 11. Steady state density distribution along the converging–diverging nozzle.

The shock location history is shown in Figure 13 for CFL numbers of 0.3, 0.5, 0.7 and 0.85. Maximum deviation between steady state shock locations for different CFL numbers is 0.12% of the nozzle length. The largest deviation with respect to exact shock position is 0.33% of

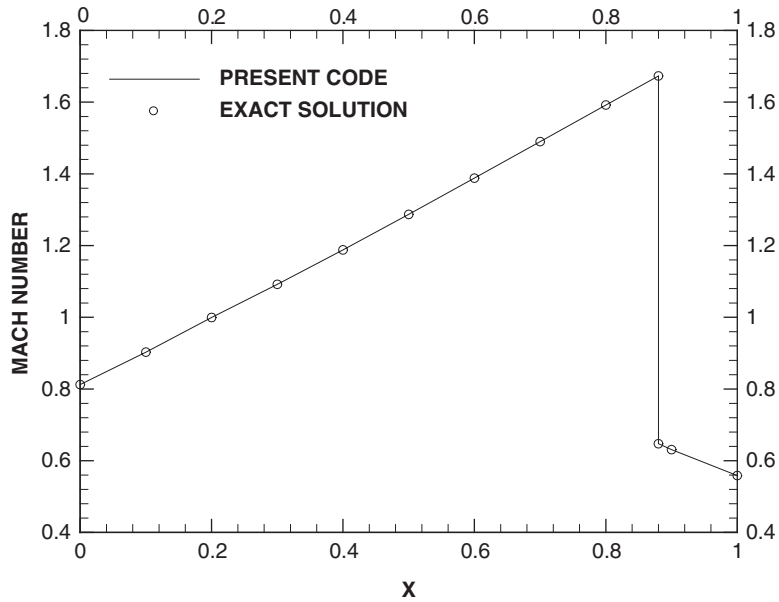


Figure 12. Steady state velocity distribution along the converging–diverging nozzle.

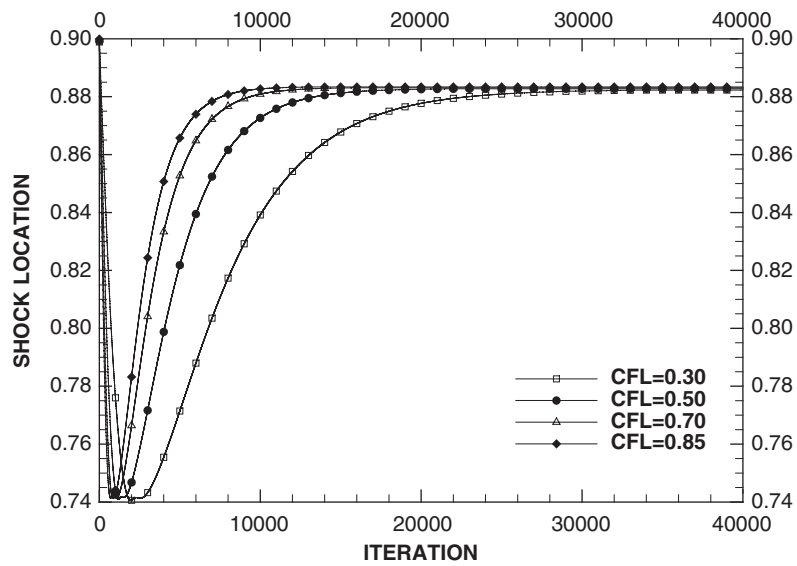


Figure 13. Shock location history for different CFL numbers.

the nozzle length which is encountered for CFL = 0.85. Sharp shock geometry, correct shock location and correct shock jump demonstrates that shock tracking and shock correction are managed accurately by the present method.

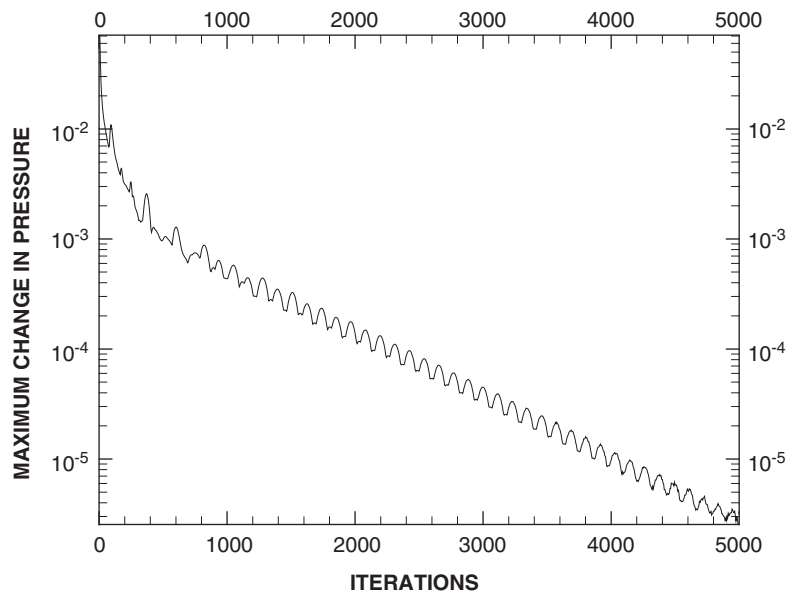


Figure 14. Convergence history.

5.3. Sinusoidal Bump (2D)

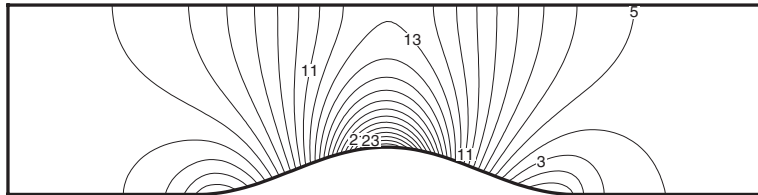
The flow in a two-dimensional duct with a sinusoidal bump is calculated for an inlet Mach number of 0.39. The duct contour is sinusoidal and symmetric about the throat. The area ratio of the throat is 0.75, and the upstream and downstream areas are equal. The computational grid used in this study has 161×41 nodes whereas the sinusoidal portion has 81×41 nodes.

Far field (characteristic) boundary conditions are employed by imposing the constant value of Q_∞ (and a zero value of θ along the upstream boundary and the constant value of R_∞ along the downstream boundary. The solution converges after about 5500 iterations with a CFL number of 0.50 (see Figure 14). The calculated Mach number and flow angle contours by the present code and that of Verhoff [12] are shown in Figures 15–18. Mach number distributions along the lower and upper walls are shown in Figure 19. The contour lines and wall distributions are symmetric about the throat, which indicates the solution accuracy.

5.4. 3D Supersonic flow in a constant area duct

The three-dimensional duct flow with square cross section is calculated for an inlet Mach number of 2. A $41 \times 41 \times 41$ grid with cubic cells is used for the 3D geometry which is practically a cube.

On both inflow and outflow surfaces, characteristic boundary conditions are applied. At the inflow boundary, the Riemann variables Q and R , modified entropy S , inlet flow angles θ and ϕ are specified explicitly. At the outflow boundary, no physical boundary conditions are specified, but numerical boundary conditions are calculated based on the information defined by the inner flow.



Level	M
25	0.7230
23	0.6905
21	0.6581
19	0.6256
17	0.5932
15	0.5607
13	0.5282
11	0.4958
9	0.4633
7	0.4309
5	0.3984
3	0.3659
1	0.3335

Figure 15. Mach number contours.

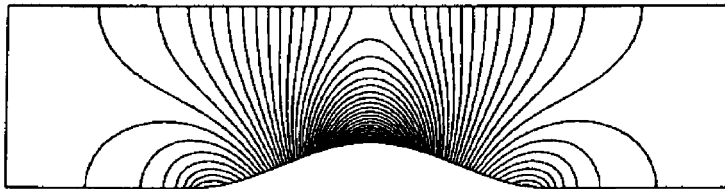
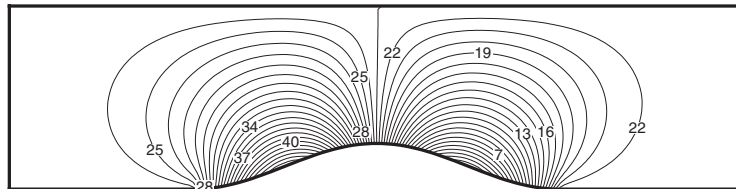


Figure 16. Reference Mach number contours [12].



Level	TH
43	0.3249
40	0.2761
37	0.2274
34	0.1787
31	0.1299
28	0.0812
25	0.0325
22	-0.0162
19	-0.0650
16	-0.1137
13	-0.1624
10	-0.2112
7	-0.2599
4	-0.3086
1	-0.3573

Figure 17. Flow angle (θ) contours (in radians).

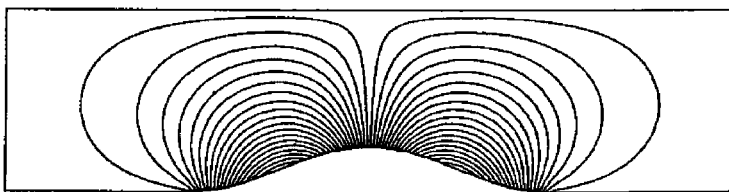


Figure 18. Reference flow angle (θ) contours [12].

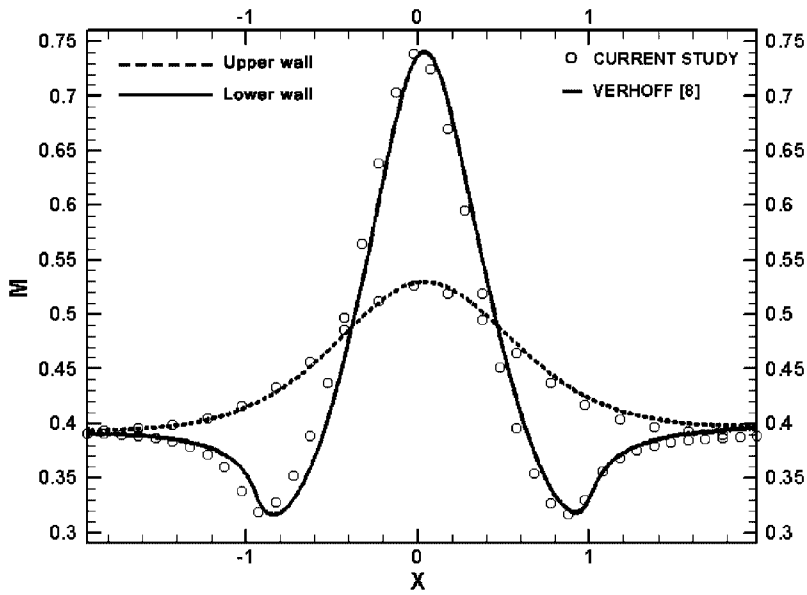


Figure 19. Mach number distribution along the walls.

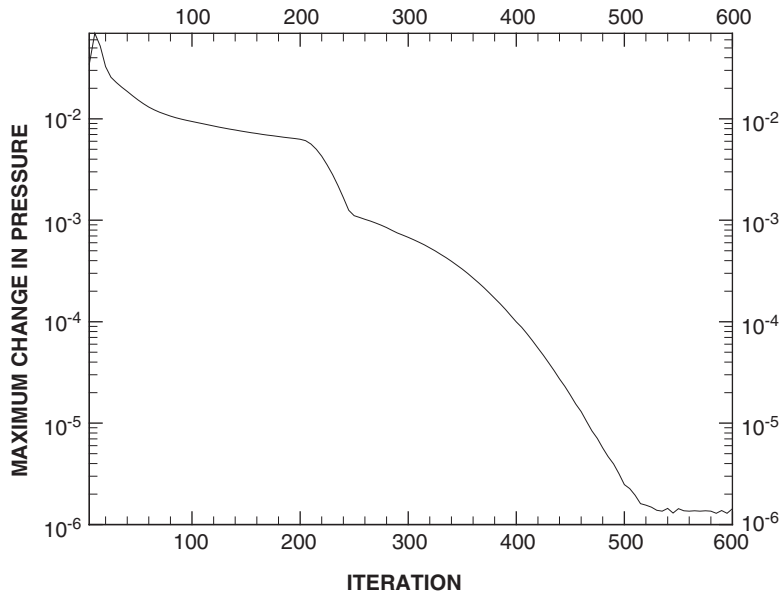
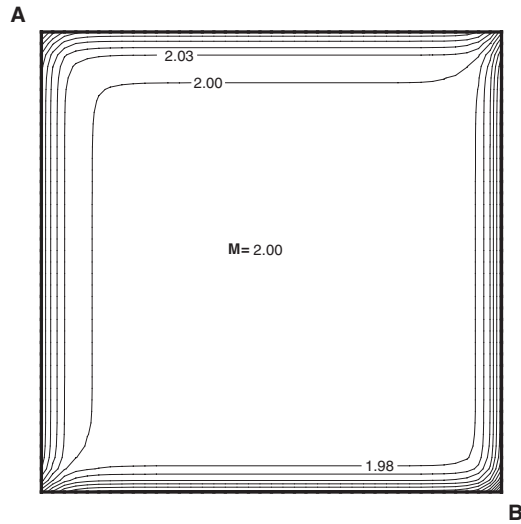
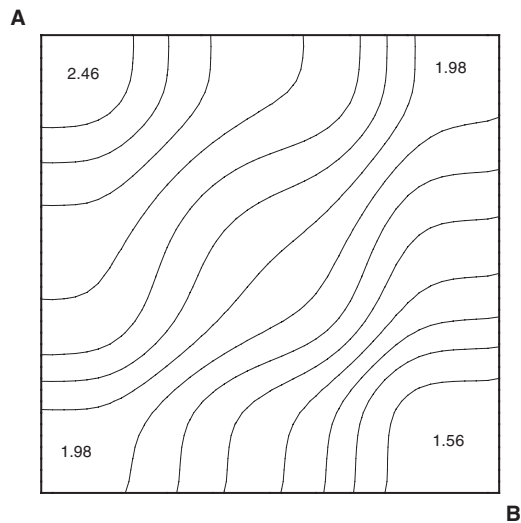


Figure 20. Convergence history.

The inlet flow angles were $\theta = -6^\circ$ and 6° . Thus, the flow is expected to be symmetric about the diagonal $A-B$. The solution converges after about 300 iterations with a CFL number of 0.50 (see Figure 20).

Figure 21. Mach contours at $x/L = 0.025$.Figure 22. Mach contours at $x/L = 0.50$.

Mach contours at various axial stations along the duct are shown in Figures 21–23. As expected the flow is symmetric about the diagonal $A-B$. The oblique shock surface forming on the lower and side surfaces of the duct, interact to create the symmetry about the diagonal. The shocks obtained by the present method are in close agreement with those presented by Verhoff [13] (see Figure 24).

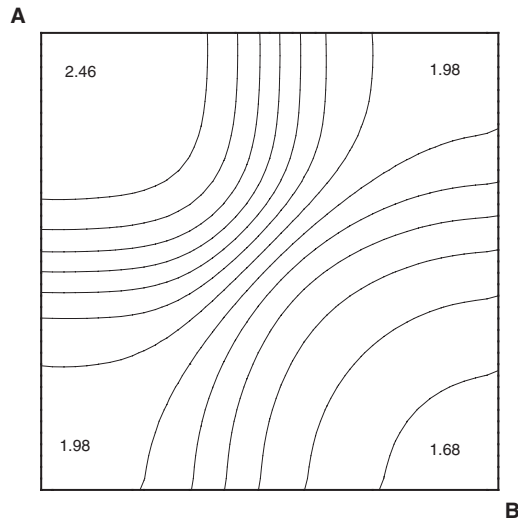


Figure 23. Mach contours at $x/L = 0.975$.

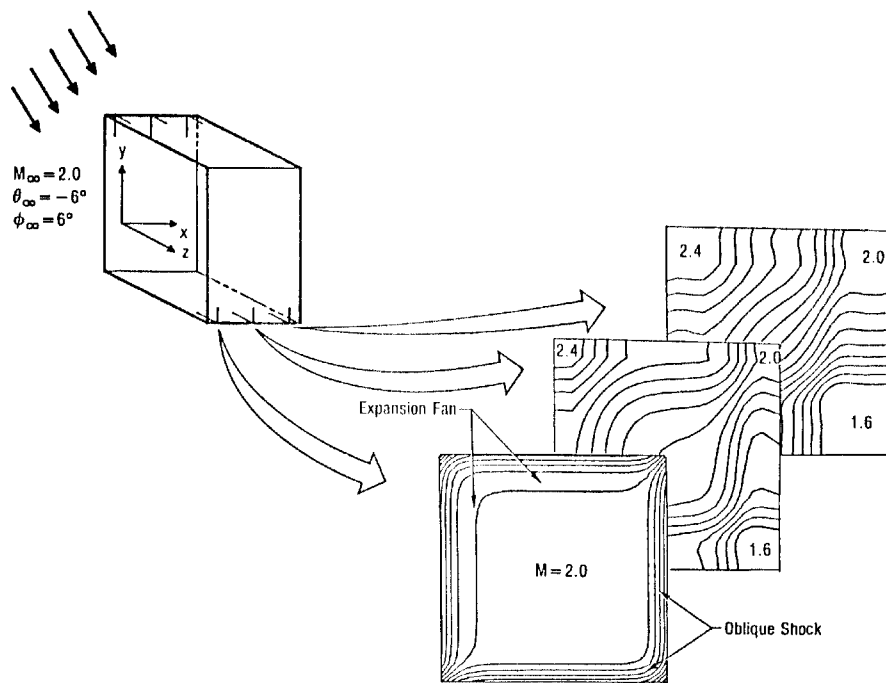


Figure 24. Mach contours [13].

6. CONCLUSION

A characteristic Euler algorithm is developed for the solution of high-speed internal flows. The equations are expressed in local streamline co-ordinate system and are written in terms of extended Riemann variables. In this form, Euler equations become a quasi-one-dimensional system regardless of the number of spatial dimensions. Subsonic, transonic and supersonic flows can be handled equally well.

A classical shock tube problem was solved to test and demonstrate the accuracy of the unsteady wave motion and shock fitting approach. The discontinuity location and the jump in flow parameters across the discontinuities are found to be in close agreement with the analytical solution. The quasi-one-dimensional transonic flow in a Laval nozzle is then solved to show that the discontinuity location within the nozzle is calculated accurately.

The two-dimensional subsonic flow over a sinusoidal bump was solved to show the capability and accuracy in handling subsonic flows. In this regard, the contour symmetry about the throat is successfully calculated. Finally, a three-dimensional supersonic flow in a constant area duct is calculated. In this simple geometry, oblique shocks and expansion fans are formed due to inlet flow angles. The results are successfully compared with available numerical solution.

NOMENCLATURE

a	speed of sound
CFL	Courant–Friedrich–Lewy number
m	unit vector normal to the streamline and n -direction
n	unit vector normal to the streamline direction (in the plane defined by the y -axis and s vector)
p	pressure
P	logarithm of pressure ($P \equiv \ln(p)$)
Q	modified Riemann variable ($Q \equiv q + aS$)
q	flow speed
R	modified Riemann variable ($R \equiv q - aS$)
S	modified entropy $\left(dS \equiv -\frac{1}{\gamma} \frac{dQ}{T} \right)$ [6]
s	unit vector in the streamline direction
t	time
w	vector of the principle variables, Q, R, S, θ, ϕ
x	spatial variable
y	spatial variable
z	spatial variable
	vector of the right-hand sides of the governing equations

Greek symbols

∂	partial derivative operator
Δt	time step

ϕ	flow angle
γ	ratio of specific heats
η	spatial variable in the computational domain
λ	characteristic (eigenvalue)
	the slope of characteristic trajectory in the space–time plane
θ	flow angle
ρ	density
ξ	spatial variable in the computational domain
ζ	spatial variable in the computational domain

Subscripts

i	node index (along x direction)
j	node index (along y direction)
k	node index (along z direction)
m	m -derivative (normal)
n	n -derivative (normal)
s	s -derivative (streamwise)
t	time derivative
x	x -component or x -derivative
y	y -component or y -derivative
z	z -component or z -derivative
η	η -derivative
ξ	ξ -derivative
ζ	ζ -derivative

Superscripts

n	n th time level
	normal
T	transpose of the matrix

REFERENCES

1. Sod GA. *Numerical Methods in Fluid Dynamics*. Cambridge University Press: Cambridge, 1985.
2. Thornhill CK. The numerical method of characteristics for hyperbolic problems in three independent variables. *Aeronautical Research Council R&M* No. 2615, September 1948.
3. Holt M. The method of characteristics for steady supersonic rotational flow in three dimensions. *Journal of Fluid Mechanics* 1956; **1**(4):409.
4. Moretti G, Abbett M, A time-dependent computational method for blunt body flows. *AIAA Journal* 1966; **4**(12):2136–2141.
5. Eaton RR. Three-dimensional numerical and experimental flowfield comparisons for sphere-cones. *Journal of Spacecraft* 1970; **7**(2):203–204.
6. Verhoff A, O'Neil PJ. A natural formulation for numerical solution of the Euler equations. *AIAA Paper No. 84-0163*, January 1984.
7. Salacka TF. Review, implementation and test of the QAZ1D computational method with a view to wave rotor applications. *M.S. Thesis*, Naval Postgraduate School, Monterey, CA, December 1985.
8. Johnston DT. Further development of a one-dimensional unsteady Euler code for wave rotor applications. *M.S. Thesis*, Naval Postgraduate School, Monterey, CA, March 1987.

9. Verhoff A, O'Neil PJ, Hopping B. Euler solutions for airfoils using the QAZ1D formulation. *Proceedings of the AIAA 18th Fluid Dynamics, Plasma Dynamics and Laser Conference*, Cincinnati, Ohio, 16–18 July, 1985.
10. Agrawal S, Vermeland RE, Verhoff A, Lowrie RB. Euler transonic solutions over finite wings. *AIAA Paper No. 88-0009*, January 1988.
11. Moretti G, DiPiano MT. An improved lambda-scheme for one-dimensional flows. *NASA Contractor Report 3712*, 1983.
12. Verhoff A, Stookesberry D. Second-order, far-field computational boundary conditions for inviscid duct flow problems. *AIAA Journal* 1992; **30**(5):1268–1276.
13. Verhoff A, O'Neil PJ. A natural formulation for numerical solution of the Euler equations. *MCAIR Report 83-031*, McDonnell Aircraft Company, St. Louis, MO, December 1983.